Counter-propagating wave patterns in a swarm model with memory

Angelika Manhart

Courant Institute of Mathematical Sciences,
New York University, 251 Mercer Street,
New York, NY 10012, USA

November 13, 2019

Abstract

Hyperbolic transport-reaction equations are abundant in the description of movement of motile organisms. Here, we focus on a system of four coupled transport-reaction equations that arises from an age-structuring of a species of turning individuals. By modeling how the behavior depends on the time since the last reversal, we introduce a memory effect. The highlight consists of the explicit construction and characterization of counter-propagating traveling waves, patterns which have been observed in bacterial colonies. Stability analysis reveals conditions for the wave formation as well as pulsating-in-time spatially constant solutions.

Keywords: traveling waves, hyperbolic equations, viscous limit, myxobacteria, wave formation, age-structured equations, pattern formation

Classification: 35L60, 35Q70, 35B32, 35B35, 35B36, 35B40, 35B65, 34D20, 92D25, 92D50

1 Introduction

Large-scale patterns such as aggregation, waves or other structures created by groups of animals or microbes have always been a popular study object for mathematical modelers and analysts. Traditionally most such models for the movement of organisms were of parabolic nature, see [3, 9, 18, 22, 26]. The last two decades have seen a rise in the use of kinetic and hyperbolic models to model biological systems, see [2, 4, 14, 15, 27] (bacterial movement, [23], chemotaxis of D. discoideum, [16]), see also the review in [10]. Kinetic models are often derived as limits of individual based models (IBMs, also often called agent-based or particle models). IBMs are particularly useful if detailed experimental data, such as the speeds, tracks and interactions of the moving agents are available, as very little approximations are necessary to translate the biology into a mathematical formalism. On the other hand IBMs can typically be analyzed by direct simulation alone, limiting their

predictive and mechanistic insight (see e.g. discussion in [17, 24]).

The analysis of hyperbolic models presents different challenges, as compared to that of their diffusion containing counter-parts, one reason being the fact that resulting solutions are typically less smooth. One of the most famous of such models is the Goldstein-Kac model presented in [13, 21] for a correlated random walk in 1D: Here a particles moves with speed s to the right or the left and its change of direction is modeled as a Poisson process with constant intensity l. Denoting the density of right- and left-moving particles by $u(x,t)$ and $v(x,t)$ this yields

$$\partial_t u + s\partial_x u = lv - lu,$$
$$\partial_t v - s\partial_x v = lu - lv. \tag{1}$$

Here the reaction term is linear and it is well known that the system is equivalent to a damped wave equation for the sum of the two densities (applying the *Kac-trick*, see [21]).

Several works have described the big variety of spatio-temporal patterns that nonlinear, local and non-local variants of (1) can produce, see e.g. [10, 11], these include stationary and traveling pulses, zigzag pulses and traveling trains. In this work we focus on what has been termed ripples, a spatio-temporal pattern in which two families of densities form counter-propagating traveling waves. Each density constitutes a genuine traveling wave, i.e. wave collisions do not affect the wave profiles. Such waves have already been observed as piecewise constant functions in [23], where a nonlinear version of the Goldstein-Kac model was analyzed:

$$\partial_t u + s\partial_x u = l(u)v - l(v)u,$$
$$\partial_t v - s\partial_x v = l(v)u - l(u)v. \tag{2}$$

Here $l(\rho)$ is a density dependent turning function. This system has also been mentioned in [7] and a similar system was derived for locusts in [12]. Even for such simple models as (2) several open questions exist, such as potential blow-up behavior for quadratic l, or characterizing the limiting traveling waves for sigmoidal l. We will elucidate the latter question in Sec. 5.

However the main part of this work deals with a generalization of (2) in which an age-structuring is introduced, see [8, 10, 14].Here age-structuring refers to the use of an independent, internal variable with units of time (the "age"). Age-structuring is commonly used in population or epidemic models (see e.g. [6]), where properties of the individuals depends on their actual age. However, it has also been used in a broader sense, e.g. in neuron models, such as that presented in [28], where "age" refers to the time since the last firing, which influences a neuron's behavior. Similarly, in this work's starting point, the example of myxobacteria given in [8], the age a is the time since the last reversal and is assumed to influence the turning behavior:

$$\partial_t u + s\partial_x u + g\partial_a u = -l(V,a)u, \quad \partial_t v - s\partial_x v + g\partial_a v = -l(U,a)v, \tag{3}$$
$$u(x,0,t) = \frac{1}{g}\int_0^\infty l(U,a)v\,\mathrm{d}a, \quad U(x,t) = \int_0^\infty u(x,a,t)\,\mathrm{d}a,$$
$$v(x,0,t) = \frac{1}{g}\int_0^\infty l(V,a)u\,\mathrm{d}a, \quad V(x,t) = \int_0^\infty v(x,a,t)\,\mathrm{d}a.$$

In this model g is the rate of aging. Allowing for only two age-groups and assuming that only the group of the higher age can actually reverse allows to eliminate a as an independent variable and leads to four transport-reaction equations that are coupled through their nonlinear reaction terms (see Sec. 2 below and [8] for the derivation). We will see that also this model allows for counter-propagating traveling waves, in this case with more complex profiles than piecewise constant. However, the waves come with a twist: While their shape stays

the same, their composition in terms of the two age groups is modified by the oncoming wave.

The rest of the manuscript is organized as follows: In Sec. 2 we present the model and connect it to existing models through asymptotic scaling, in Sec. 3 we analyze the space-independent dynamics in terms of existence and stability of steady states. In particular we find a Hopf-bifurcation. We proceed in Sec. 4 to analyze the effect the transport term has on the stability of the steady states. In Sec. 5 we show the existence and construction of counter-propagating traveling waves. Finally in Sec. 6 we compare the calculated wave profiles to numerical simulations. Throughout this manuscript stability always refers to asymptotic stability.

2 Model Introduction and Scaling

The following model is a generalization of that derived and presented in [8]. We describe individuals moving in a 1D interval, $x \in [0, L]$. We denote by $u_{0/1}(x, t)$ and $v_{0/1}(x, t)$ the densities of individuals moving with speed $s > 0$ to the right and left respectively. Each group can exist in one of two states: a reversible state (subscript 1) and a non-reversible state (subscript 0), which fulfill

$$
\begin{aligned}
\partial_t u_0 + s \, \partial_x u_0 &= -g(v_0 + v_1)u_0 + l(u_0 + u_1)v_1, \\
\partial_t u_1 + s \, \partial_x u_1 &= g(v_0 + v_1)u_0 - l(v_0 + v_1)u_1, \\
\partial_t v_0 - s \, \partial_x v_0 &= -g(u_0 + u_1)v_0 + l(v_0 + v_1)u_1, \\
\partial_t v_1 - s \, \partial_x v_1 &= g(u_0 + u_1)v_0 - l(u_0 + u_1)v_1.
\end{aligned}
\tag{4}
$$

The left-hand-sides describe the (linear) transport of the densities, the right-hand-side the reactions. Individuals cycle through the different groups; starting with a non-reversible, right-moving individual we have: $u_0 \to u_1$ (particle "ages" into a reversible state), $u_1 \to v_0$ (particle reverses, thereby changes direction and becomes non-reversible), $v_0 \to v_1$ (particle "ages" into a reversible state) and finally $v_1 \to u_0$. The function $l(\rho) > 0$ describes a turning rate that depends on the total density of opposing individuals, as has been suggested in [8]. The aging function $g(\rho) > 0$ can be interpreted as the reciprocal value of a refraction period during which the individuals are unable to change their direction. It's dependence on the density of oncoming individuals presents a novelty compared to [8]. The interpretation is that the internal "clock" that determines the reversability is affected by signals coming from the opposing individuals. In general other dependencies of l and g on the densities are possible, however the procedure to construct the traveling waves in Sec. 5 might break down then. In previous works such as [8, 31], $l(\rho)$ was assumed to be sigmoidal. This shape was motivated by experiments performed with myxobacteria, where the reversal rate l was shown to exhibit a step-like dependence on the amount of signaling molecule received during head-to-head contacts with other bacteria, [30]. A density dependence of g is more speculative, but might prove useful for future applications. Here, we don't prescribe particular shapes of $l(\rho)$ and $g(\rho)$, but keep the sigmoidal shape for $l(\rho)$ and a constant $g(\rho)$ as reference examples in mind.

We equip system (4) with periodic boundary conditions. As initial average mass we define $m_0 > 0$ to be

$$
2m_0 = \frac{1}{L} \int_0^L (u_0 + u_1 + v_0 + v_1) \, \mathrm{d}x.
$$

Scaling. We use as reference time, space and density L/s, L and m_0 respectively, i.e. if $\sim$ denotes a dimensionless quantity, we set $\tilde{t} = \frac{t\,s}{L}$, $\tilde{x} = \frac{x}{L}$ and $\tilde{w} = \frac{w}{m_0}$, where w represents any of the densities. We define the dimensionless aging and reversal functions by

$$
\gamma(\tilde{w}) = \frac{L}{s} g(m_0 \tilde{w}), \quad \lambda(\tilde{w}) = \frac{L}{s} l(m_0 \tilde{w}).
$$

Finally, we drop the $\sim$, i.e. we keep the same notation for the dimensionless densities, space and time. This gives $x \in [0, 1]$ and

$$\int_0^1 (u_0 + u_1 + v_0 + v_1)\,\mathrm{d}x = 2.$$

The transformed system written in terms of $u = u_0 + u_1$ and $v = v_0 + v_1$, u_1 and v_1 reads

$$
\begin{aligned}
\partial_t u + \partial_x u &= \lambda(u)v_1 - \lambda(v)u_1, \\
\partial_t v - \partial_x v &= \lambda(v)u_1 - \lambda(u)v_1, \\
\partial_t u_1 + \partial_x u_1 &= \gamma(v)(u - u_1) - \lambda(v)u_1, \\
\partial_t v_1 - \partial_x v_1 &= \gamma(u)(v - v_1) - \lambda(u)v_1.
\end{aligned}
\tag{5}
$$

Throughout this work, we will often assume the following properties of λ and γ:

$$\gamma, \lambda \in \mathcal{C}^k([0, \infty)), \quad k \geq 2, \quad 0 < \underline{\gamma} \leq \gamma(\rho), \quad 0 < \underline{\lambda} \leq \lambda(\rho), \quad \forall \rho \geq 0.
\tag{6}$$

Limit of fast aging. To link the model in (5) to other existing models, it is instructive to look at the limit of fast aging, i.e. we set $\gamma(w) \to \frac{1}{\varepsilon}\gamma(w)$ for a small parameter ε. If we develop the densities with respect to ε, i.e.

$$
\begin{aligned}
u(x, t) &= u^0(x, t) + \varepsilon u^1(x, t) + \mathcal{O}(\varepsilon^2), \quad v(x, t) = v^0(x, t) + \varepsilon v^1(x, t) + \mathcal{O}(\varepsilon^2), \\
u_1(x, t) &= u_1^0(x, t) + \varepsilon u_1^1(x, t) + \mathcal{O}(\varepsilon^2), \quad v_1(x, t) = v_1^0(x, t) + \varepsilon v_1^1(x, t) + \mathcal{O}(\varepsilon^2),
\end{aligned}
$$

we obtain the following sets of equations: *To first order*

$$
\begin{aligned}
\partial_t u^0 + \partial_x u^0 &= \lambda(u^0)v^0 - \lambda(v^0)u^0, \\
\partial_t v^0 - \partial_x v^0 &= \lambda(v^0)u^0 - \lambda(u^0)v^0, \\
u_1^0 &= u^0, \quad v_1^0 = v^0,
\end{aligned}
\tag{7}
$$

to second order

$$
\begin{aligned}
\partial_t u^1 + \partial_x u^1 &= \left[\lambda'(u^0)v^0 - \lambda(v^0)\right]u^1 - \left[\lambda'(v^0)u^0 - \lambda(u^0)\right]v^1 \\
&\quad + \lambda(u^0)\lambda(v^0)(v^0 - u^0), \\
\partial_t v^1 - \partial_x v^1 &= \left[\lambda'(v^0)u^0 - \lambda(u^0)\right]v^1 - \left[\lambda'(u^0)v^0 - \lambda(v^0)\right]u^1 \\
&\quad + \lambda(u^0)\lambda(v^0)(u^0 - v^0), \\
u_1^1 &= u^1 - \frac{\lambda(u^0)}{\gamma(v^0)}v^0, \quad v_1^1 = v^1 - \frac{\lambda(v^0)}{\gamma(u^0)}u^0.
\end{aligned}
$$

The model without aging (7) (also termed *memory-free model*) has been described already e.g. in [8, 23]. In this model all individuals are always in a reversible state. Already in [23] it has been observed that, for certain choices of λ, this model produces piecewise-constant counter-propagating waves. We will revisit (7) in Sec. 5, where we'll show some new properties.

3 The space-independent dynamics

Before dealing with the effect of the transport operator, we study the space-independent system, which constitutes a system of four coupled nonlinear ODEs for $(u(t), v(t), u_1(t), v_1(t))$. Since $u(t) + v(t) \equiv 2$, we can rewrite

the system in terms of only three equations, for $d(t) = (u(t) - v(t))/2$, $u_1(t)$ and $v_1(t)$.

$$\dot{d} = \lambda(1 + d)v_1 - \lambda(1 - d)u_1, \tag{8}$$
$$\dot{u}_1 = \gamma(1 - d)(1 + d - u_1) - \lambda(1 - d)u_1,$$
$$\dot{v}_1 = \gamma(1 + d)(1 - d - v_1) - \lambda(1 + d)v_1.$$

The next two lemmata collect some straight forward properties.

Lemma 3.1. *Let* $\gamma, \lambda \in \mathcal{C}^k([0, \infty))$ $k \geq 2$ *and assume that there exist constants* $\underline{\lambda}, \underline{\gamma} > 0$, *such that*

$$\underline{\gamma} \leq \gamma(\rho), \quad \underline{\lambda} \leq \lambda(\rho), \quad \forall \rho \geq 0.$$

An (isotropic) steady state of (8) *is given by*

$$d = 0, \quad u_1 = v_1 = \frac{\gamma(1)}{\gamma(1) + \lambda(1)}. \tag{9}$$

A sufficient condition for the existence of an additional pair of steady states is given by

$$\tau := \frac{\gamma(1)}{\lambda(1)} \left[\lambda'(1) - \lambda(1) \right] + \frac{\lambda(1)}{\gamma(1)} \left[\gamma'(1) - \gamma(1) \right] > 0. \tag{10}$$

Proof. By solving the steady state equations of u_1 and v_1 for u_1 and v_1 respectively and substituting the expressions into the steady state equation for d, it is easy to see that finding steady states of (8) is equivalent to finding $\bar{d} \in [-1, 1,]$ such that $\bar{d}$ is a root of

$$G(d) = (1 - d)Q_+(d) - (1 + d)Q_-(d), \quad Q_\pm(d) = \frac{\lambda(1 \pm d)\gamma(1 \pm d)}{\lambda(1 \pm d) + \gamma(1 \pm d)}$$

The remaining values are then given by

$$u_1 = \frac{\gamma(1 - \bar{d})}{\gamma(1 - \bar{d}) + \lambda(1 - \bar{d})}(1 + \bar{d}), \quad v_1 = \frac{\gamma(1 + \bar{d})}{\gamma(1 + \bar{d}) + \lambda(1 + \bar{d})}(1 - \bar{d}). \tag{11}$$

The fixed point associated to $G(0) = 0$ is the isotropic steady state in (9). Since G is continuous, $G(d) = G(-d)$ and $G(1) < 0$, a sufficient condition for the existence of two additional roots of G is $G'(0) > 0$, which is equivalent to $\tau > 0$. $\qquad\square$ $\qquad\qquad\square$

Lemma 3.2. *Let the assumptions of Lem.* 3.1 *hold.*

a. *The (isotropic) steady state of* (8) *given by* (9) *is stable iff the following two conditions hold*

1. $\tau < 0$, *where* τ *is defined in* (10),
2. $\lambda'(1) < 2\lambda(1)$, *or*

$$\gamma(1) \notin [\lambda'(1) - \lambda(1) - \Omega, \lambda'(1) - \lambda(1) + \Omega], \Omega := \sqrt{\lambda'(1)(\lambda'(1) - 2\lambda(1))}$$

b. *A necessary condition for the stability of any non-isotropic steady state* $\bar{d} \neq 0$, *is* $G'(\bar{d}) < 0$.

Proof. Part a: Linearizing around (9) yields a matrix whose characteristic polynomial is given by

$$p(z) = (z + l + g)\left[z^2 + (l + g - 2b)z + 2(lg - bg - lc)\right] \tag{12}$$

$$l = \lambda(1), \quad g = \gamma(1), \quad b = \lambda'(1)\frac{\gamma(1)}{\gamma(1) + \lambda(1)}, \quad c = \gamma'(1)\frac{\lambda(1)}{\gamma(1) + \lambda(1)}. \tag{13}$$

The eigenvalue $z = -l - g$ is always negative. For the remaining quadratic polynomials the Routh-Hurwitz criterion asserts that stability is equivalent to the positivity of both coefficients, which in turn is equivalent to the first claim of the lemma.

Part b: Let $0 \neq \bar{d} \in [-1, 1]$ be such that $G(\bar{d}) = 0$, which is equivalent to

$$\bar{d} = \frac{Q_+ - Q_-}{Q_+ + Q_-}.$$

Here and in the following we always evaluate all functions at $d = \bar{d}$. Using this, we can write

$$G'(\bar{d}) = 2\frac{Q'_+ Q_- - Q'_- Q_+}{Q_+ + Q_-} - (Q_+ + Q_-),$$

where $'$ denotes the derivative w.r.t. to d. Linearizing around the non-isotropic steady state given by $\bar{d}$ and (11) yields a matrix whose determinant, using the expression for $G'(\bar{d})$ derived above, can be written as

$$\left(\lambda(1 + \bar{d}) + \gamma(1 + \bar{d})\right)\left(\lambda(1 - \bar{d}) + \gamma(1 - \bar{d})\right)G'(\bar{d}),$$

Since the determinant of a 3×3 matrix is minus the constant term of the corresponding characteristic polynomial, the Routh-Hurwitz theorem requires it to be negative for stability. This finishes the proof of part b. □ □

It is noteworthy that the second condition in Lemma 3.2 allows for a situation where there exists only the isotropic steady state, but it is unstable. This indicates a more complicated long-term behavior, such as limit cycles, as demonstrated in the following example:

Example 3.1. Hopf bifurcation. *We use the following expressions for $\lambda(\rho)$ and $\gamma(\rho)$,*

$$\lambda(\rho) = \underline{\lambda} + \frac{\overline{\lambda} - \underline{\lambda}}{1 + \exp\left(-\alpha(\rho - 1)\right)}, \quad \gamma(\rho) \equiv \gamma, \tag{14}$$

and interpret $\gamma > 0$ as bifurcation parameter. $\lambda(\rho)$ is a sigmoid function taking values between $\underline{\lambda}$ and $\overline{\lambda}$. It has its steepest gradient, characterized by α, at $\rho = 1$. We define $\lambda_\pm = \frac{\overline{\lambda} \pm \underline{\lambda}}{2} > 0$. To ensure that the first alternative of condition 2 in Lem. 3.2, part a is always violated we choose $\alpha > 4\lambda_+/\lambda_-$. Expressing the remaining conditions in terms of γ now yields that the isotropic steady state is stable iff the following two conditions hold

1. $\gamma < \dfrac{2\lambda_+^2}{\alpha\lambda_- - 2\lambda_+} =: \hat{\gamma}$

2. $\gamma \notin \left[\underbrace{\dfrac{\alpha\lambda_- - 2\lambda_+ - \sqrt{\alpha\lambda_-(\alpha\lambda_- - 4\lambda_+)}}{2}}_{=:\gamma^*}, \underbrace{\dfrac{\alpha\lambda_- - 2\lambda_+ + \sqrt{\alpha\lambda_-(\alpha\lambda_- - 4\lambda_+)}}{2}}_{=:\gamma^{**}}\right]$

Note that our choice of α also ensures that $\gamma^* < \hat{\gamma} < \gamma^{**}$. Finally we'd like to ensure that the sufficient condition for existence of a non-isotropic steady state of Lemma 3.1 is also necessary. An easy way to do this is to choose $\lambda_+ > \lambda_-\sqrt{3}$ or equivalently $\overline{\lambda} < (2 + \sqrt{3})\underline{\lambda}$. This can be checked easily, details are omitted. At the bifurcation point $\gamma = \gamma^*$, the isotropic fixed point becomes unstable and the pair of complex conjugated eigenvalues passes
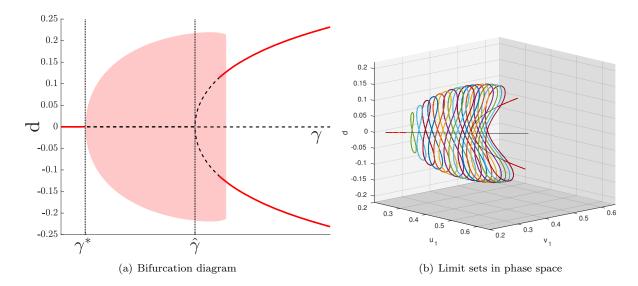
| (a) Bifurcation diagram | (b) Limit sets in phase space |

Figure 1: *Hopf bifurcation.* (a) Shown is the bifurcation diagram for the parameter γ using the limiting values of d to represent the solution. Stable steady states are indicated by solid red lines, unstable steady states by dashed black lines. The region where a limit cycle is stable is shown in pale red. (b) The corresponding limit sets in (u_1, v_1, d)-space. Stable and unstable steady states are shown in thick red and thin black respectively, periodic limit cycles in many colors. Parameters are $(\underline{\lambda}, \overline{\lambda}, \alpha) = (2.5, 8, 10)$, yielding $(\gamma^*, \hat{\gamma}, \gamma^{**}) = (1.82, 3.24, 15.18)$. As initial conditions small perturbations from the isotropic steady state were used.

through the imaginary axis, i.e. we have a supercritical Hopf bifurcation. The resulting limit cycle represents spatially homogeneous colonies of bacteria that periodically-in-time change the fraction of right and left moving bacteria. The author is not aware of corresponding behaviors in applications. However, such a phenomenon might also be difficult to observe e.g. under the microscope, since the total density $u + v$ remains constant. Numerical tests showed that the pulsating solutions are not stable, if space dependency is included.

Fig. 1 shows the bifurcation diagram and the limiting behavior of (8) obtained by varying γ. For future work it would be interesting to study the stability of the limit cycle and the non-isotropic fixed points. Here, we only note that examination of the eigenvalues of the linearization around the non-isotropic steady state indicate that its change in stability (see Fig. 1a for $\gamma > \hat{\gamma}$) is caused by a pair of complex eigenvalues crossing the imaginary axis. However, no additional limit-cycles are observed, indicating that the genericity condition of a Hopf bifurcation is violated, see e.g. [25].

4 Space-Homogeneous Steady States

A typical starting point of understanding pattern formation is to investigate the stability of space-homogeneous steady states. Their existence and values are discussed in Lem. 3.1 and their stability in the space-independent system is discussed in Lem. 3.2. Next we discuss how the transport operator affects these stability criteria.

Proposition 4.1. *Let $\gamma, \lambda \in \mathcal{C}^k([0, \infty))$ $k \geq 2$ and assume that there exist constants $\underline{\lambda}, \underline{\gamma} > 0$, such that*

$$\underline{\gamma} \leq \gamma(\rho), \quad \underline{\lambda} \leq \lambda(\rho), \quad \forall \rho \geq 0.$$

a. Let $(\bar{u}, \bar{v}, \bar{u}_1, \bar{v}_1)$ be the isotropic space-homogeneous steady state given by (9). Assume that

$$0 < \lambda'(1) < \lambda(1), \quad \gamma'(1) < \gamma(1). \tag{15}$$

7

Then $(\bar{u}, \bar{v}, \bar{u}_1, \bar{v}_1)$ is linearly stable. If $\lambda'(1) > \lambda(1)$, it is always unstable.

b. *Let $\tau > 0$ hold and let $(\bar{u}, \bar{v}, \bar{u}_1, \bar{v}_1)$ be the non-isotropic space-homogeneous steady state given by (10). Necessary conditions for its linear stability are*

$$\lambda'(\bar{u})\bar{v}_1 < \frac{\gamma(\bar{v})\lambda(\bar{v})}{\gamma(\bar{v}) + \lambda(\bar{v})}, \quad \lambda'(\bar{v})\bar{u}_1 < \frac{\gamma(\bar{u})\lambda(\bar{u})}{\gamma(\bar{u}) + \lambda(\bar{u})}, \quad G'(\bar{u} - \bar{v}) < 0$$

Proof. We only show the proof of part a, part b uses the same techniques, but since it involves the use of the Routh Hurwitz criterion for complex polynomials, the calculations become somewhat cumbersome. We linearize around the first steady state with perturbations of zero total mass. Using matrix notation and calling the perturbations $r(x, t) \in \mathbb{R}^4$ we obtain the linear system

$$\partial_t r + T \partial_x r = Mr, \quad T = \begin{pmatrix} 1 & 0 & 0 & 0 \\ 0 & -1 & 0 & 0 \\ 0 & 0 & 1 & 0 \\ 0 & 0 & 0 & -1 \end{pmatrix}, \quad M = \begin{pmatrix} b & -b & -l & l \\ -b & b & l & -l \\ g & c-b & -g-l & 0 \\ c-b & g & 0 & -g-l \end{pmatrix},$$

where l, g, b and c are defined as in the proof of Lem. 3.2. To asses the behavior of the system we look at perturbations of the form

$$r(x, t) = r_0 \, e^{\xi t + i k x}, \quad k = 2\pi n, \quad n \in \mathbb{Z}, w_0 \in \mathbb{R}^4 \backslash \{0\},$$
$$\text{yielding} \quad (M - T i k) \, r_0 = \xi r_0.$$

Expressing (15) in terms of l, g, b and c gives

$$0 < b < \frac{g \, l}{g + l}, \quad c < \frac{g \, l}{g + l}. \tag{16}$$

Hence we need to determine under what conditions $A = M - T i k$ has only eigenvalues ξ with negative real part for all k. We use the Routh-Hurwitz criterion for the (fourth order) characteristic polynomial of A, p_A. This yields the following conditions in terms of the the coefficients of $p_A(x) = x^4 + a_3 x^3 + a_2 x^2 + a_1 x + a_0$, where $a_i = a_i(g, l, b, c, k)$.

1. $a_i > 0$

2. $p = a_3 a_2 - a_1 = p_1 k^2 + p_0 > 0$

3. $q = a_3 a_2 a_1 - a_1^2 - a_3^2 a_0 = q_1 k^2 + q_0 > 0$

where

$$a_0 = k^2 (k^2 + g^2 + l^2 + 2l(b - c)), \tag{17}$$
$$a_1 = 2 \left[k^2 (g + l - b) + (g + l)(g \, l - b \, g - c \, l) \right],$$
$$a_2 = 2k^2 + (g + l)(g + l - 2b) + 2(g \, l - b \, g - c \, l), \quad a_3 = 2(g + l - b),$$
$$p_0 = 2(g + l - 2b) \left[(g + l)(g + l - b) + g \, l - b \, g - c \, l \right], \quad p_1 = 2(g + l - b),$$
$$q_0 = 4(g + l)(g \, l - b \, g - c \, l)(g + l - 2b) \left[(g + l)(g + l - b) + g \, l - b \, g - c \, l \right],$$
$$q_1 = 16(g + l - b)^2 \left[g \, l - b(g + l) \right]$$

It is easy to see that (16) implies

$$g \, l - b \, g - c \, l > 0, \quad g + l - 2b > 0, \tag{18}$$

and with the coefficients expressed as in (17) this shows that (16) implies stability. On the other hand if $b > \frac{g \, l}{g + l}$, $q_1 < 0$ and hence we have instability for large k. $\square$ $\square$

Remark 4.1. *Comparing Prop. 4.1 to Lem. 3.2 we see that the stability criteria for the ODE system are necessary, but not sufficient for the space-dependent system. A crucial difference is the additional requirement that*

$$\lambda'(1) < \lambda(1),$$

which makes it possible to choose functions $\lambda(\rho)$ and $\gamma(\rho)$ and parameter regimes where the destabilization of the isotropic steady state requires the transport operator.

Example 4.1. Constant aging function. *For density independent aging functions $\gamma(\rho) \equiv \gamma$, criterion $\lambda'(1) < \lambda(1)$ becomes both necessary and sufficient for the stability of the isotropic state. In such a case the reversal function λ needs to have super-linear growth at 1 for the isotropic state to destabilize and the destabilization is independent of γ. In [8], where such a model was applied to myxobacterial movement, two wave forming criteria were determined numerically. The authors used a growing, piecewise quadratic, sigmoidal $\lambda(\rho)$, characterized by a minimal value λ_m, a maximal value λ_M and an inflection density $\bar{\rho}$. Translating criterion (15) back to dimensional variables yields $\lambda'(m_0)m_0 < \lambda(m_0)$, and applying it to the model in [8] gives as destabilization conditions*

$$\lambda_M - 3\lambda_m > 0, \quad \frac{2\lambda_m}{\lambda_M - \lambda_m} < \frac{m_0}{\bar{\rho}} < \frac{2(\lambda_M - 2\lambda_m)}{\lambda_M - \lambda_m}.$$

Hence we recover the two wave formation criteria observed in [8]: The maximal reversal rate needs to be large enough compared to the minimal reversal rate and the average total density needs to be close to the inflection density.

5 Counter-propagating Traveling Waves

Upon simulation of the full system (5) (see also Sec. 6) a typical observed behavior is the formation of counter-propagating traveling waves for the two total densities $u(x,t)$ and $v(x,t)$. We therefore introduce the following definition.

Definition 5.1. *We call any solution (u, v, u_1, v_1) of (5) a **Counter-propagating Traveling Wave Solution** with speed $\pm c$, if there exist functions $P(\xi)$ and $M(\eta)$, such that*

$$u(x,t) = P(x - ct), \quad v(x,t) = M(x + ct).$$

This section is devoted to showing the existence of such waves and explicitly constructing their shapes. For the memory-free system (7) we also present some new stability results.

5.1 Waves in the Memory-free System

Before analyzing the age-dependent system (5) we aim to understand the waves in the memory-free system (7). By a slight abuse of notation we call the densities of right-moving and left-moving individuals again u and v, i.e. we look at

$$\begin{aligned}
\partial_t u + \partial_x u &= \lambda(u)v - \lambda(v)u, \\
\partial_t v - \partial_x v &= \lambda(v)u - \lambda(u)v.
\end{aligned} \tag{19}$$

equipped with periodic boundary conditions on $[0, 1]$ and $\int_0^1 (u + v) \, dx = 2$. This system has already been discussed in [23, 31]. Here we will summarize their findings and add a new result concerned with the stability of traveling waves.
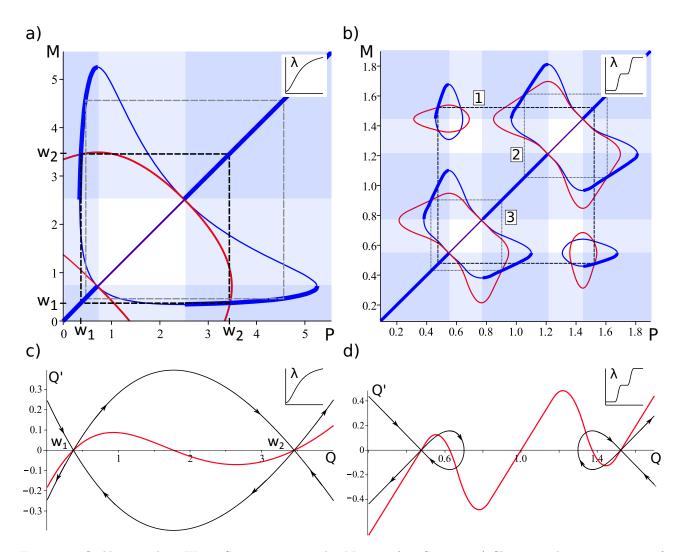
Figure 2: *Stable Traveling Wave Construction in the Memory-free System.* a) Shown is the construction of stable candidate values of piecewise traveling waves in the memory-free system (19) in $(u, v) = (P, M)$ space. The turning function used is described in Ex. 5.2 and shown in the inset. Pairs of values that are roots of the right-hand-side in (19) (condition **A** in Rem. 5.2) are shown in solid blue. Blue shading represents the linear stability condition (condition **B** in Rem. 5.2), thick blue lines mark linearly stable pairs. Finally the integral condition **C** is shown in red. The selected pair is depicted as thick dashed black square, a linearly stable pair (not selected by the viscous limit) is shown in thin-dashed gray. b) Construction of stable candidate values for Ex. 5.3. The turning function $\lambda(\rho)$ used is shown in the inset. Linestyles and colors as in a), dashed black squares numbered 1, 2 and 3 represent three potentially stable pairs. c) For the pair (w_1, w_2) selected by the construction in a) the heteroclinic orbit in (Q, Q')-space is shown. This corresponds to the selected solution to the fast equation (24). The inset shows the corresponding $\lambda(\rho)$. d) As c), but for Ex. 5.3. The turning function $\lambda(\rho)$ used is shown in the inset. The (homoclinic) orbit in (Q, Q') space shown corresponds to the pair marked by 1 in b).

10

Construction and linear stability. We seek counter-propagating traveling waves in the sense of Def. 5.1 of speed ± 1. Making the ansatz $u(x,t) = P(x-t), v(x,t) = M(x+t)$ and defining as wave frames $\xi = x - t$ and $\eta = x + t$, one finds the condition

$$\frac{P(\xi)}{\lambda(P(\xi))} = \frac{M(\eta)}{\lambda(M(\eta))} \equiv r > 0. \tag{20}$$

Fig. 2a,b shows all such solutions (blue curve) for a sigmoid or double-sigmoid $\lambda(\rho)$. For any given constant r, condition (20) will generically allow for only a finite set of possible values $I_r := \{w_1, \ldots w_K\}$ that P and M can take, i.e. $P, M : [0,1] \to I_r$, hence any counter-propagating traveling wave has to be piecewise constant. When assessing the linear stability of such waves, the simultaneous existence of two traveling waves frame provides a challenge and in general wouldn't allow for a standard perturbation ansatz. However, a work-around is to assume one density to be completely constant (say $M(\eta) \equiv M$); now an ansatz in the frame of the other wave can be used, i.e.

$$u(\xi, t) = P(\xi) + \varepsilon \tilde{u}(\xi, t), \quad v(\xi, t) = M(\xi) + \varepsilon \tilde{v}(\xi, t),$$

for perturbations $\tilde{u}$ and $\tilde{v}$. Looking at the spectrum of the associated linear operator yields as stability condition (confer [31])

$$\lambda'(w_i)w_i < \lambda(w_i), \tag{21}$$

for any $w_i \in I_r$. An important observation is that r parametrizes a whole family of stable tuples I_r (compare Fig. 2a,b, thick blue lines), however upon simulation only a particular tuple associated to a particular value of r seems to be selected (Fig. 3). Note that also the (conserved) total mass cannot explain this selection since by shifting the jump points the mass can be varied without changing the wave heights. In the following we argue that the observed selection is driven by a small diffusion term, introduced by the numerical scheme. However, as explained below, for many applications, including the bacterial swarms that originally motivated this system, the inclusion of a small amount of density diffusion is in fact necessary to accurately describe the underlying particle dynamics.

Selection via diffusive regularization. Already in [8] it has been noted that a small amount of density diffusion is necessary to be in agreement with the underlying particle model. If the density diffusion term is omitted, the derived continuum system can produce traveling waves of arbitrarily small wavelengths, contradicting the original particle model, where the wavelengths seem to be controlled. The derivation of the continuum model involves the expansion of an interaction operator in terms of a dimension-less quantity, the ratio between the interaction radius of the bacteria and the spatial scales of the macroscopic phenomena of interest (the waves). Biological parameters indicate that this ratio is small, but not very small. Hence it appears that the correct approximation of the interaction operator has to include order-one terms (Chapman-Enskog expansion, see [5]), which leads to the density diffusion introduced here. Motivated by this, we therefore add a small diffusion term to (19) for $0 < \varepsilon << 1$

$$\begin{aligned} \partial_t u + \partial_x u &= \lambda(u)v - \lambda(v)u + \varepsilon^2 \partial_x^2 u, \\ \partial_t v - \partial_x v &= \lambda(v)u - \lambda(u)v + \varepsilon^2 \partial_x^2 v. \end{aligned} \tag{22}$$

Now we let $\varepsilon \to 0$ and consider the values selected by (22) to be the "correct" ones. A similar procedure was also applied e.g. in [1]. Let now $\{w_1, \ldots, w_K\} = I_r$ be a linearly stable solution tuple, i.e. fulfill (21) and for a fixed $r > 0$

$$\frac{w_i}{\lambda(w_i)} = r, \quad \forall i = 1 \ldots K.$$

11

We set $v(x,t) = M(x+t) \equiv w_1$ and search for solutions $u(x,t) = P(x-t) = P(\xi)$ of the first equation in (22). We introduce a fast scale $\zeta = \xi/\varepsilon$ and define $Q(\zeta) = P(\xi)$. Substituting this into (22) yields

$$0 = \lambda(P)w_1 - \lambda(w_1)P + \varepsilon^2 P'' \xrightarrow{\varepsilon \to 0} 0 = \lambda(P)w_1 - \lambda(w_1)P, \tag{23}$$

$$0 = \lambda(Q)w_1 - \lambda(w_1)Q + Q''. \tag{24}$$

We already know that for $\varepsilon \to 0$ on the slow scale P will take values in I_r. Since we want to understand jumps between values in I_r, we search for solutions Q that form a heteroclinic orbit connecting w_1 with any other $w_i \in I_r$, $i \neq 1$. Multiplying (24) with Q' and integrating with respect to ζ now yields

$$C = \int^Q (\lambda(u)w_1 - \lambda(w_1)u) \; \mathrm{d}u + \frac{1}{2}(Q')^2, \tag{25}$$

for some constant C. Since we require $Q(\zeta) \to w_1$ and $Q(\zeta) \to w_i$ for $\zeta \to \pm\infty$, we obtain the integral condition

$$\int^{w_1} (\lambda(u)w_1 - \lambda(w_1)u) \; \mathrm{d}u = \int^{w_i} (\lambda(u)w_1 - \lambda(w_1)u) \; \mathrm{d}u. \tag{26}$$

This constitutes a necessary condition for "correct" tuples.

Remark 5.1. Concerning the wave speeds. *The above procedure requires that the traveling waves of the diffusive system travel with speed 1, independent of ε. If instead we were to search for solutions with speed $1 - \varepsilon\theta$, it would be possible to show the existence of heterogeneous orbits for a larger class of tuples I_r, in contradiction with the numerical results. Determining why an ε-independent wave speed is the right choice, will be subject of future work.*

Remark 5.2. Alternative formulation and summary. *We can rewrite (26) as follows: By dividing the right-hand-side of (26) by w_1 and evaluating the second part of the integral we get*

$$\int^{w_i} \lambda(u)\,\mathrm{d}u - \frac{\lambda(w_1)}{w_1}\frac{w_i^2}{2}.$$

Since the fraction $\lambda(w_1)/w_1 = \lambda(w_i)/w_i$ for all $w_i \in I_r$, we can replace it in the second term and obtain a formulation that is independent of w_1. We can now summarize the procedure to construct candidate values for stable (i.e. linearly stable and selected by the limit $\varepsilon \to 0$ in (22)) counter-propagating traveling waves as follows: Defining

$$\Lambda(\rho) = \frac{\rho}{\lambda(\rho)}, \quad \Omega(\rho) = \int_0^\rho \lambda(u)\,\mathrm{d}u - \frac{\lambda(\rho)\rho}{2}, \tag{27}$$

any stable tuple $\{w_1, \ldots, w_K\}$ has to fulfill $\forall i, j \in \{1, \ldots K\}$

$$\boldsymbol{A}: \; \Lambda(w_i) = \Lambda(w_j), \quad \boldsymbol{B}: \; \Lambda'(w_i) > 0, \quad \boldsymbol{C}: \; \Omega(w_i) = \Omega(w_j).$$

Note that $\boldsymbol{B}$ is just a reformulation of (21). The sought solutions to (19) are now of the form $u(x,t) = P(x-t)$, $v(x,t) = M(x+t)$ with $P(\xi), M(\eta) \in \{w_1, ..w_K\}$. Fig. 2 and Ex. 5.2, 5.3 (below) illustrate this construction.

The following lemma provides an easy way to find stable values for a class of turning functions $\lambda(\rho)$. In particular it applies to many sigmoid turning functions.

Lemma 5.2. Anti-symmetric turning function. *Let $\lambda(\rho)$ be anti-symmetric with respect to some density $\bar{\rho} > 0$ in the following sense: There exist $0 < \underline{\lambda} < \overline{\lambda}$ such that*

$$\overline{\lambda} - \lambda(\bar{\rho} + \rho) = \lambda(\bar{\rho} - \rho) - \underline{\lambda}, \quad \forall \rho \in [-\bar{\rho}, \bar{\rho}]. \tag{28}$$

Then a stable pair of values (w_1, w_2) can be found by replacing condition $\boldsymbol{C}$ in Rem. 5.2 with
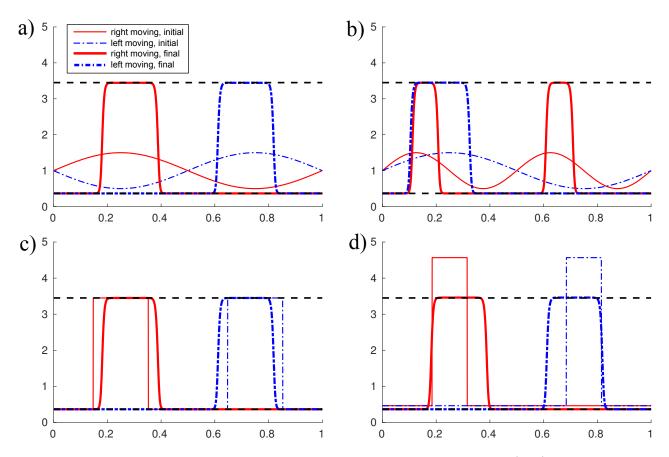
$$w_2 = 2\bar{\rho} - w_1.$$

12

Figure 3: *Long-term Behavior of the Memory-free System.* Shown are the initial values (thin) and the simulation outcome at time $t = 98$ (thick) for four different initial conditions, a)-d). u, the right-moving density is shown in solid-red, v, the left-moving density in dashed-dotted blue. The constructed stable values w_1, w_2 from Fig. 2a) are shown as horizontal black dashed lines. d) corresponds to the pair shown in dashed gray in Fig. 2a). We used $\Delta x = 6.25 \times 10^{-4}$ and a time step of $\Delta t = 6.06 \times 10^{-4}$ (compare Sec. 6).

Proof. Let $w_2 = 2\bar{\rho} - w_1$. We start by observing that condition **A** together with (28) implies that

$$\Lambda(w_1) = \Lambda(w_2) = \frac{2\bar{\rho}}{\overline{\lambda} + \underline{\lambda}}. \tag{29}$$

Performing a change of variables $u \to 2\bar{\rho} - u$ and using (28) it is easy to see that

$$\hat{\Omega}(w) := \int_{\bar{\rho}}^{w} (\lambda(u)w_1 - \lambda(w_1)u)\ \mathrm{d}u$$
$$= \hat{\Omega}(2\bar{\rho} - w) + (\bar{\rho} - w)\left[2\bar{\rho}\lambda(w_1) - (\overline{\lambda} + \underline{\lambda})w_1\right]$$
$$= \hat{\Omega}(2\bar{\rho} - w),$$

where we have used (29) in the last line. Noting that condition **C** is equivalent to $\hat{\Omega}(w_1) = \hat{\Omega}(w_2)$ finishes the proof. $\qquad\square$ $\qquad\qquad\qquad\qquad\qquad\qquad\qquad\qquad\square$

13

Example 5.1. Linear and quadratic turning functions. *If $\lambda(\rho) = a + b\rho$, i.e. linear, the reaction term is equivalent to that obtained using a constant turning function $\lambda(\rho) = a$, since the terms involving b cancel. In this case (19) reduces to the Goldstein-Kac model (1) mentioned in the introduction and no waves can be formed ($\Lambda(\rho) = \rho/\lambda(\rho)$ is injective). If $\lambda(\rho) = a + b\rho^2$ is quadratic, non-trivial pairs fulfilling condition $\mathbf{A}$ in Rem. 5.2 can be found as $u\,v = a/b$, however the larger of the two values will always violate condition $\mathbf{B}$.*

Example 5.2. Sigmoid turning function. *We demonstrate the construction for a sigmoid turning function for which $\Lambda(\rho)$ changes sign twice. We use $\lambda(\rho) = \underline{\lambda} + (\overline{\lambda} - \underline{\lambda})\alpha\rho^2/(1 + \alpha\rho^2)$ with $\underline{\lambda} = 0.5$, $\overline{\lambda} = 10$, $\alpha = 0.125$. Note that this choice of turning function does not fulfill (28). Fig. 2a shows how stable counter-propagating traveling waves (in the sense of Rem. 5.2) are constructed: Using the definitions of Λ and Ω given in (27), one seeks the intersections of the implicitly defined curves*

$$\Lambda(u) = \Lambda(v), \quad \Omega(u) = \Omega(v)$$

in (u, v)-space (show in blue and red respectively) for which $\Lambda' > 0$ (blue shading in Fig. 2a). To confirm the obtained values (w_1, w_2) we simulated (19) for various initial conditions shown in Fig. 3, thin lines. The final traveling profiles are shown in Fig. 3, thick lines and confirm the analytically determined stable pair (w_1, w_2). Fig. 2c shows that for the fast system (24) this indeed corresponds to a heteroclinic orbit connecting w_1 and w_2.

Example 5.3. Double-sigmoid turning function. *A non-trivial example where not all constructed values are actually stable is given by a double-sigmoid function, parametrized by $\underline{\lambda} < \hat{\lambda} < \overline{\lambda}$, $0 < \underline{\rho} < \overline{\rho}$ and $0 < \delta < \min\left\{\underline{\rho}, \frac{\overline{\rho} - \underline{\rho}}{2}\right\}$ and shown in the inset in Fig. 2b.*

$$\lambda(\rho) = \begin{cases} \underline{\lambda} & \rho < \underline{\rho} - \delta \\ \underline{\lambda} + \frac{\hat{\lambda} - \underline{\lambda}}{2\delta^2}\left(\rho - \underline{\rho} + \delta\right)^2 & \underline{\rho} - \delta \le \rho < \underline{\rho} \\ \hat{\lambda} - \frac{\hat{\lambda} - \underline{\lambda}}{2\delta^2}\left(\rho - \underline{\rho} - \delta\right)^2 & \underline{\rho} \le \rho < \overline{\rho} - \delta \\ \hat{\lambda} & \underline{\rho} + \delta \le \rho < \overline{\rho} - \delta \\ \hat{\lambda} + \frac{\overline{\lambda} - \hat{\lambda}}{2\delta^2}\left(\rho - \overline{\rho} + \delta\right)^2 & \overline{\rho} - \delta \le \rho < \overline{\rho} \\ \overline{\lambda} - \frac{\overline{\lambda} - \hat{\lambda}}{2\delta^2}\left(\rho - \overline{\rho} - \delta\right)^2 & \overline{\rho} \le \rho < \overline{\rho} + \delta \\ \overline{\lambda} & \rho \ge \overline{\rho} + \delta. \end{cases}$$

We use as parameters $(\underline{\lambda}, \hat{\lambda}, \overline{\lambda}) = (2.5, 5.25, 8)$, $(\underline{\rho}, \overline{\rho}) = (0.67, 1.33)$ and $\delta = 1/6$. Inspection of the curves defined by Ω and Λ show three possible pairs of stable values, marked by 1,2,3 in Fig. 2b. However in light of the conserved average mass of one, pairs 2 and 3 would lead to a too low and too high overall mass respectively, hence cannot be candidates for long-term behavior. For the remaining pair 1, the orbit in phase-space shown in Fig. 2d shows that it does not constitute the sought after heteroclinic orbit connecting the two states. Consequently we expect to find no stable piecewise constant traveling waves for this choice of turning function, this was confirmed numerically.

5.2 Traveling Waves in the Full System

In this section we construct traveling waves for the full system (5) for arbitrary aging and turning functions. We start by noting that Def. 5.1 does not refer to u_1 and v_1. The main result of this section is to postulate specific dependencies of u_1 and v_1 on the traveling wave frames $x \pm ct$ and be thus able to derive closed, decoupled equations for the wave profiles.

Construction. We seek counter-propagating traveling wave solutions moving with speed ± 1. We expect that the composition of a wave in terms of reversible and non-reversible individuals is modified by the opposing

wave. This motivates the introduction of the functions $A(x,t) = u_1(x,t)/u(x,t)$ and $B(x,t) = v_1(x,t)/v(x,t)$, i.e. the ratios of reversible individuals within a right- and left moving wave respectively. We now postulate that $A(x,t)$ depends only on $x + t$ and $B(x,t)$ only on $x - t$, i.e. the traveling wave frame of the *opposing* group. The ansatz can be summarized as

$$u(x,t) = P(x-t), \quad u_1(x,t) = P(x-t)A(x+t)$$
$$v(x,t) = M(x+t), \quad v_1(x,t) = M(x+t)B(x-t). \tag{30}$$

Substituting this into (5) and assuming that A and B are bounded away from zero, we find that $P(\xi)$, $M(\xi)$, $A(\eta)$ and $B(\eta)$ have to fulfill

$$\frac{P(\xi)}{\lambda(P(\xi))B(\xi)} = \frac{M(\eta)}{\lambda(M(\eta))A(\eta)} = r, \tag{31}$$

for some $r > 0$, and

$$2\,A'(\eta) = \gamma(M(\eta))\,[1 - A(\eta)] - \lambda(M(\eta))A(\eta) \tag{32}$$
$$-2\,B'(\xi) = \gamma(P(\xi))\,[1 - B(\xi)] - \lambda(P(\xi))B(\xi).$$

Remark 5.3. Decoupling of the Wave Frames. *Classically, when searching for traveling waves, the use of a traveling wave ansatz facilitates the reduction to one or several ordinary differential equations. However, for families of* counter-propagating *traveling waves, this procedure doesn't work, since the two wave frames would typically interact with each other. The key consequence of the above ansatz is the decoupling for the frames $\eta = x + t$ and $\xi = x - t$, thereby yielding a system of ODEs and algebraic equations. Note that this requires very particular structural properties. If, e.g. λ or γ were to be functions also of the other density (as suggested e.g. in [23]), the procedure would break down.*

It is important to note that (30) does not constitute a modeling assumption, but an ansatz motivated by numerical observations and intuition. While the mathematical usefulness of this ansatz is obvious – it decouples the wave frames – its validity will be demonstrated numerically in Sec. 6. In the following we will only refer to $P(\xi)$ and $B(\xi)$, since $M(\eta)$ and $A(\eta)$ can be treated analogously. If we analyze (31) and (32) in the (P, B) plane, we see that the dynamics can be described with the aid of two functions and their associated curves

$$\Lambda(\rho) = \frac{\rho}{\lambda(\rho)}, \quad \Gamma(\rho) = \frac{\gamma(\rho)}{\gamma(\rho) + \lambda(\rho)} \tag{33}$$

$$\rho \mapsto \Lambda_c^r(\rho) := (\rho, \Lambda(\rho)/r), \quad \rho \mapsto \Gamma_c(\rho) := (\rho, \Gamma(\rho)) \tag{34}$$

Condition (31) means that $(P(\xi), B(\xi))$ has to lie on Λ_c^r for all ξ. The dynamic on this curve is described by (32), where the direction of the dynamic, i.e. the sign of B' is determined by whether $(P(\xi), B(\xi))$ is above Γ_c, i.e. $B' > 0$, or below, then $B' < 0$. Fig 4 summarizes the construction, details can be found in the proof of Prop. 5.4.

Remark 5.4. *Wherever $P \in \mathcal{C}^2$, equations (31) and (32) can be combined to one ordinary differential equation for P,*

$$P' = \frac{\lambda(P)\,[P(\lambda(P) + \gamma(P)) - \lambda(P)\gamma(P)r]}{2\,(\lambda(P) - P\lambda'(P)))}. \tag{35}$$

As noted in Prop. 5.4, P will in general not be continuous everywhere (compare Fig. 4b). Note that the values where P jumps do not correspond to the singularities of its derivative, i.e. singularities of the right-hand-side of (35). In fact, as the more insightful construction using B (discussed above and in the caption of Fig. 4) shows, several solutions with different jumps can exist. Future stability analysis of the constructed waves might shed light on how to identify those jump points which correspond to stable waves.
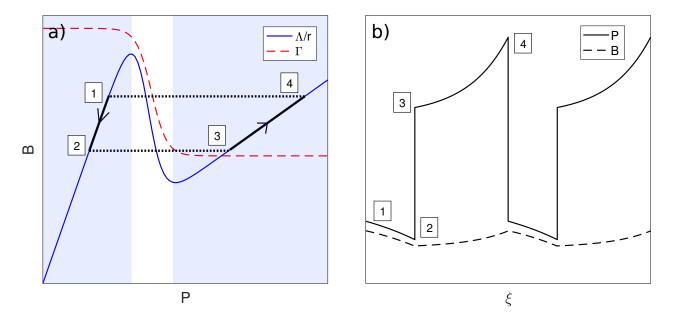
15

Figure 4: *Construction of Traveling Waves.* a) Construction of admissible solutions in the sense of Def. 5.3 in $(P, B) = (u, v_1/v)$ space (left) and the corresponding solutions $P(\xi), B(\xi)$ (right). Left: Solutions have to lie on Λ_c^r (solid blue) for some fixed $r > 0$. The curve Γ (dashed red) divides the space according to the sign of B'. The white region marks non-admissible areas. $1 \to 2$: Since $B < \Gamma$, $B' < 0$ and we move downwards along Λ_c^r. $2 \to 3$: We jump from one admissible branch to another one (dotted), B does not change its value, but P does. $3 \to 4$: Now $B > \Gamma$ and thereby $B' > 0$ and we move along Λ_c^r. $4 \to 1$: We again jump horizontally in (P, B) space back to the original branch (dotted). Right: The corresponding solutions $P(\xi)$ and $B(\xi)$, numbers refer to the corresponding numbers in (P, B) space in the left figure.

We will see in Sec. 6 that the constructed waves can be observed as long-term limits of the simulated densities, indicating that at least some are stable. In this work we do not deal with the stability of the traveling waves, however motivated by the stability results in Sec.4 and the observed numerical behavior, we only focus on one class of waves, which we will call *admissible* (see Def. 5.3). We expect that all stable waves will be admissible, however a proof (or dis-proof) will be the subject of future work. Before stating the existence result, we therefore introduce the following useful definitions.

Definition 5.3. *Admissibility and Reachability. Let $\rho > 0$, $I \subset [0, \infty)$ and Λ given by (33).*

1. *We call ρ **admissible**, if $\Lambda'(\rho) > 0$ ($\iff$ $\lambda'(\rho)\rho < \lambda(\rho)$).*

2. *We define the **reachability set** of ρ, $\mathcal{R}_\rho$ and that of I, $\mathcal{R}_I$ by*

$$\mathcal{R}_\rho := \{\rho^* > 0 \,|\, \rho^* \neq \rho, \, \Lambda(\rho) = \Lambda(\rho^*), \, \rho^* \text{ admissible}\}, \quad \mathcal{R}_I := \bigcup_{\rho \in I} \mathcal{R}_\rho.$$

   *If $\mathcal{R}_\rho \neq \emptyset$ we call ρ **reachable**.*

3. *We call a pair of functions $0 < P(\xi)$ and $0 < B(\xi) \leq 1$ **admissible solution** if there exists an $r > 0$ such that they solve (31), (32) and there exists $\bar{\xi} > 0$ such that $B(0) = B(\bar{\xi})$, $P(0) = P(\bar{\xi})$ and $P(\xi)$ is admissible for all $\xi \in [0, \bar{\xi}]$.*
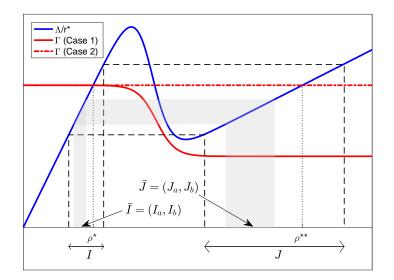
16

Figure 5: *Proof of Existence.*

The following proposition shows the existence of admissible, counter-propagating waves and details several properties. The most notable is that P is necessarily discontinuous.

Proposition 5.4. *Let $\gamma, \lambda \in \mathcal{C}^k([0,\infty))$ $k \geq 2$ and assume that there exist constants $\underline{\lambda}, \underline{\gamma} > 0$, such that*

$$\underline{\gamma} \leq \gamma(\rho), \quad \underline{\lambda} \leq \lambda(\rho), \quad \forall \rho \geq 0.$$

Further assume that there exist values $0 < \rho_1 < \rho_2 < \rho_3$ such that

$$\begin{cases} \Lambda'(\rho) > 0 & \rho \in (0, \rho_1) =: I_1 \\ \Lambda'(\rho) < 0 & \rho \in (\rho_1, \rho_2) \\ \Lambda'(\rho) > 0 & \rho \in (\rho_2, \rho_3) =: I_2. \end{cases}$$

Then there exists an admissible solution in the sense of Def. 5.3, $B \in \mathcal{C}([0,\infty))$ and piecewise in $\mathcal{C}^k([0,\infty))$ and P piecewise in $\mathcal{C}^k([0,\infty))$, but $P \notin \mathcal{C}([0,\infty))$. For all values $\hat{\xi} \in [0,\infty)$ where B and P are not in $\mathcal{C}^k$, P fulfills the jump condition

$$\lim_{\xi \to \hat{\xi}+} \frac{P(\xi)}{\lambda(P(\xi))} = \lim_{\xi \to \hat{\xi}-} \frac{P(\xi)}{\lambda(P(\xi))}.$$

Proof. Please refer to Fig. 5 for an illustration of the the proof. Since $\Lambda(0) = 0$ and Λ makes at least two changes in direction, we can find open intervals $I = (a, b) \subset I_1$ and $J \subset I_2$, such that

$$\Lambda(I) = \Lambda(J)$$

We choose I and J such that their interval ends do not include local extrema of Λ. We now search for admissible solutions, with $P(\xi) \in I \cup J$ for all $\xi > 0$. We claim that it is always possible to find $r > 0$, such that

$$\Gamma(\rho) = \Lambda(\rho)/r \tag{36}$$

17

has a solution $\rho \in I$. This can be seen easily by noting that if we define

$$r_1 = \frac{\Lambda(a)}{\Gamma(a)}, \quad r_2 = \frac{\Lambda(b)}{\Gamma(b)}$$

the intermediate value theorem applied to $\rho \mapsto \frac{\Gamma(\rho)}{\Lambda(\rho)}$ together with the continuity of γ and λ ensures that (36) has a solution $\rho \in (a, b)$ for each

$$r \in (\min\{r_1, r_2\}, \max\{r_1, r_2\}) =: R_1.$$

We require that for admissible solutions $B \leq 1$. In light of (31), we therefore require $r \in (\Lambda(b), \infty) =: R_2$. Since $\Lambda(b) < r_2$,

$$R_1 \cap R_2 =: R \neq \emptyset$$

and we denote by r^* an element in R and define ρ^* by $\Gamma(\rho^*) = \Lambda(\rho^*)/r^*$. W.l.o.g. we assume that Γ crosses Λ/r^* at ρ^* (as opposed to just touching it), hence the sign of B' in (32) changes at $P = \rho^*$. Due to our construction of I and J there exists a $\rho^{**} \in J$ with $\Lambda(\rho^*) = \Lambda(\rho^{**})$.

Case 1: If $\Gamma(\rho^{**}) \neq \Lambda(\rho^{**})/r^*$, we can find subintervals $\bar{I} = (I_a, I_b) \subset I$ and $\bar{J} = (J_a, J_b) \subset J$ such that

$$\Lambda(\bar{I})/r^* = \Lambda(\bar{J})/r^*$$

and B' in (32) has opposite signs for $P \in \bar{I}$ and $P \in \bar{J}$. We assume $B' < 0$ in $\bar{I}$ and $B' > 0$ in $\bar{J}$. In light of Rmk. 5.4 we can then define an admissible solution by

1. Set $P(0) = I_b$, solve (35) with $r = r^*$ until $P(\xi_1) = I_a$ for some $\xi_1 > 0$.

2. Set $P(\xi_1) = J_a$ and solve (35) with $r = r^*$ until $P(\bar{\xi}) = J_b$ for some $\bar{\xi} > \xi_1 > 0$.

3. Define $B(\xi) = \Lambda(P(\xi))/r^*$.

This procedure works since on $\bar{I}$ and $\bar{J}$ we have $\lambda(\rho) > \rho\lambda'(\rho)$ and $\mathrm{sign}P' = \mathrm{sign}B'$. Further we can bound

$$P' \leq -\hat{P}_{\bar{I}} < 0 \text{ on } \bar{I}, \quad P' > \hat{P}_{\bar{J}} > 0 \text{ on } \bar{J}, \quad \text{where}$$

$$\hat{P}_W = \frac{\underline{\lambda}^2(\underline{\lambda} + \underline{\gamma})r^*}{2\sup_{Q \in W}(\lambda(Q) - Q\lambda'(Q))} \inf_W |\Lambda/r^* - \Gamma| > 0,$$

hence we will be able to reach I_a and J_b for finite ξ_1 and $\bar{\xi}$. Whenever P doesn't jump it is the classical solution of an ODE with the right hand side in $\mathcal{C}^{k-1}$, hence away from discontinuities of P, we have $P, B \in \mathcal{C}^k$. Further since $\Lambda(I_a) = \Lambda(J_a)$ and $\Lambda(I_b) = \Lambda(J_b)$, the resulting B will be continuous.

Case 2: If $\Gamma(\rho^{**}) = \Lambda(\rho^{**})/r^*$ we define

$$B(\xi) \equiv \Lambda(\rho^*)/r^*, \quad P \text{ piecewise constant with } P(\xi) \in \{\rho^*, \rho^{**}\}.$$

Since $\Lambda(\rho^*)/r^*$ is a fixpoint of (32), B fulfills (32) trivially and we have defined an admissible solution. $\square$ $\square$

Lemma 5.5. Bounds. *Let the assumptions of Prop. 5.4 hold and let P, B be admissible solutions in the sense of Def. 5.3. Further let*

$$\overline{P} := \max\left\{\{\rho_M\} \cup \mathcal{R}_{\rho_M} | \Lambda'(\rho_M) = 0, \ \Lambda''(\rho_M) < 0, \ \rho_M \text{ is reachable}\right\}, \tag{37}$$

$$\underline{P} := \min\left\{\{\rho_M\} \cup \mathcal{R}_{\rho_M} | \Lambda'(\rho_M) = 0, \ \Lambda''(\rho_M) > 0, \ \rho_M \text{ is reachable}\right\}. \tag{38}$$

Then we have

$$\underline{P} \leq ||P||_\infty \leq \overline{P}.$$

For the fraction B we can conclude that

$$\inf_{\rho \in [0, \infty)} \Gamma(\rho) \leq ||B||_\infty \leq \sup_{\rho \in [0, \infty)} \Gamma(\rho) < 1.$$

18

Proof. The proof consists of simple geometrical arguments using the construction depicted in Fig. 4. The bounds of P result from examining $\Lambda(\rho)$ in terms of reachability, disregarding $\Gamma(\rho)$. The borders of reachable intervals are determined by the minima and maxima of $\Lambda(\rho)$. The bounds of B are a result of the observation that the solution curve in (P, B) has to be able to jump to a branch of $\Lambda(\rho)/r$ with opposite sign of B'. □ □

Example 5.4. A simple sigmoidal λ. *To apply the construction to a simple case we set $\gamma(\rho) \equiv \gamma$ and use the simplest continuous approximation of a sigmoid $\lambda(\rho)$ given by*

$$\lambda(\rho) = \begin{cases} \underline{\lambda} & \rho < 1 - \varepsilon \\ \underline{\lambda} + \frac{\rho - 1 + \varepsilon}{2\varepsilon}(\overline{\lambda} - \underline{\lambda}) & 1 - \varepsilon \le \rho < 1 + \varepsilon \\ \overline{\lambda} & else. \end{cases} \tag{39}$$

Here $\varepsilon > 0$ is a small parameter, for $\varepsilon \to 0$ $\lambda(\rho)$ would converge to a piecewise constant function. Strictly speaking λ doesn't fulfill the smoothness requirements of Prop. 5.4, however the result could easily be generalized to continuous functions, so we may still proceed. The instability condition (15) requires

$$\varepsilon < \frac{\overline{\lambda} - \underline{\lambda}}{\overline{\lambda} + \underline{\lambda}}$$

to allow for admissible counter-propagating traveling waves. Application of Lem. 5.5 gives

$$\frac{\underline{\lambda}}{\overline{\lambda}}(1 + \varepsilon) < P < \frac{\overline{\lambda}}{\underline{\lambda}}(1 - \varepsilon), \quad \frac{\gamma}{\gamma + \overline{\lambda}} < B < \frac{\gamma}{\gamma + \underline{\lambda}},$$

Further, referring to the constant r in (31) and Prop. 5.4, we can conclude that

$$\frac{\gamma + \underline{\lambda}}{\gamma\overline{\lambda}}(1 - \varepsilon) < r < \frac{\gamma + \overline{\lambda}}{\gamma\underline{\lambda}}(1 + \varepsilon).$$

Shapes. *We apply the construction in Prop. 5.4 using (35) to obtain the following wave crest and trough shape: Let $P_{c,0} > r\frac{\gamma\overline{\lambda}}{\gamma + \overline{\lambda}}$ and $P_{t,0} < r\frac{\gamma\underline{\lambda}}{\gamma + \underline{\lambda}}$ be the initial densities of the crest and trough respectively, then*

$$P_{crest}(\xi; P_{c,0}) = r\frac{\gamma\overline{\lambda}}{\gamma + \overline{\lambda}} + e^{\frac{\gamma + \overline{\lambda}}{2}\xi}\left(P_{c,0} - r\frac{\gamma\overline{\lambda}}{\gamma + \overline{\lambda}}\right)$$

$$P_{trough}(\xi; P_{t,0}) = r\frac{\gamma\underline{\lambda}}{\gamma + \underline{\lambda}} + e^{\frac{\gamma + \underline{\lambda}}{2}\xi}\left(P_{t,0} - r\frac{\gamma\underline{\lambda}}{\gamma + \underline{\lambda}}\right).$$

In particular wave crest are convex and wave troughs are concave. When connecting wave crests with troughs, the continuity of B leads to a jump conditions for P at the discontinuity ξ_c

$$\lim_{\xi \to \xi_c-} P(\xi) = \left(\overline{\lambda}/\underline{\lambda}\right) \lim_{\xi \to \xi_c+} P(\xi) \quad \text{from crest to trough}$$

$$\lim_{\xi \to \xi_c-} P(\xi) = \left(\underline{\lambda}/\overline{\lambda}\right) \lim_{\xi \to \xi_c+} P(\xi) \quad \text{from trough to crest}$$

In particular we get for a wave with a crest for $\xi \in [0, \xi_1]$, then followed by a trough for $\xi \in [\xi_1, \xi_2]$

$$P(\xi) = \begin{cases} P_{crest}(\xi; P_{c,0}), & 0 < \xi < \xi_1 \\ P_{trough}(\xi - \xi_1; P_{t,0}), & \xi_1 < \xi < \xi_2 \end{cases},$$

$$\text{where} \quad P_{t,0} = P_{crest}(\xi_1, P_{c,0})\left(\underline{\lambda}/\overline{\lambda}\right).$$

Requiring the wave to be periodic, i.e. $B(\xi_2) = B(0)$ or equivalently $P(\xi_2) = P_{c,0}\left(\underline{\lambda}/\overline{\lambda}\right)$ yields an expression for $P_{c,0}$ in terms of ξ_1 and ξ_2. If one additionally fixes the mass of the wave, also r is determined. Fig. 6b) shows that the analytically calculated shape matches the numerically obtained one almost perfectly.
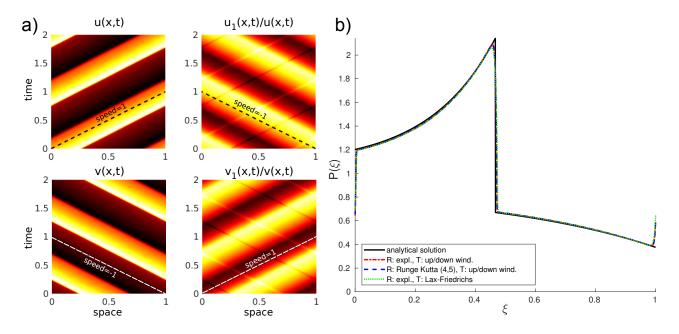
Figure 6: *Traveling Wave Frames & Shapes.* a) Space-time plots for the densities $(u, u_1/u, v, v_1/v) = (P, A, M, B)$ for a simulation using the sigmoid turning from Ex. 3.1. As initial conditions the isotropic steady state was perturbed with a sine-wave. Shown is the result for the time $t \in [48, 50]$. Colors represent high (white) and low (black) densities. Dashed lines make speed$= \pm 1$. b) Comparison between the analytically calculated and numerically determined wave shapes for different numerical schemes. We used the simple sigmoid turning function $\lambda(\rho)$ of Ex. 5.4, which allows for explicit calculation of $P(\xi)$ (solid-black). The only fitting parameter is the jump position ξ_1, which was estimated from the numerically calculated shapes. We used $(\overline{\lambda}, \underline{\lambda}, \gamma) = (2.5, 8, 1)$ and a steepness parameter $\varepsilon = 0.1$ and let the simulation run until $T = 15$. As initial condition we used the isotropic steady state perturbed with a sine wave with period one and chose the right-and left moving groups to be symmetric to each other. This created symmetric traveling waves with only one wave crest/trough and mass one, making direct comparison with the analytical solution easy. The schemes for the transport (T) and reaction (R) operator are explained in the legend.

6   Simulations

Numerical Method and Wave Shapes.   We simulated model (5) in one space dimension with periodic boundary conditions. The transport and reaction terms were implemented using operator splitting with explicit upwind or downwind (for the right- and left moving family respectively) finite differences for the transport term and an explicit treatment of the reaction term. We also tested implementing the reaction term with an explicit Runge-Kutta (4,5) formula using the ode45 solver of Matlab and a Lax-Friedrichs Scheme for the transport term. Using the analytically calculated wave shapes of Ex. 5.4 as reference, we could not observe any gain in accuracy using the more complicated schemes. Fig. 6b shows the wave shapes comparing the three different schemes, all of which lead to almost identical wave shapes that match the analytically calculated shape extremely well. We used a spatial step of $\Delta x = 6.25 \times 10^{-4}$ and a time step of $\Delta t = 6.1875 \times 10^{-4}$ which leads to only a very small amount of numerical diffusion introduced through the discretization of the transport term.

Confirmation of Traveling Wave Frames.   The crucial assumption that allowed for the construction of the traveling waves for system (5) was that both u and v_1/v form traveling waves with speed 1 to the right (and
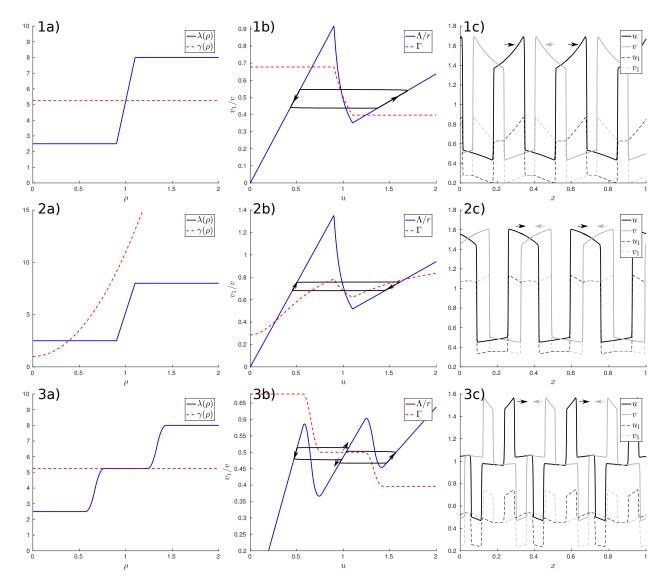
Figure 7: *Wave Gallery.* Depicted are three example choices of $\lambda(\rho)$ and $\gamma(\rho)$ (first column, letter a), the corresponding wave construction in $(P, B) = (u, v_1/v)$-space (middle column, letter b, arrows mark directions) and the resulting simulated waves (last column, letter c). Example 1: Constant $\gamma(\rho)$ and piecewise linear $\lambda(\rho)$. Wave crests increase in travel direction, wave troughs decrease. Example 2: Quadratic $\gamma(\rho)$ and piecewise linear $\lambda(\rho)$. Now wave crests decrease in travel direction, wave troughs increase. Example 3: Constant $\gamma(\rho)$ and $\lambda(\rho)$ having a triple-step shape. Wave shapes are more complicated with four piecewise smooth segments. As initial conditions in all cases I used the isotropic steady state plus a sine/cosine wave.

the left for v and u_1/u). We demonstrate the validity of this ansatz by examining the space-time evolution for the sigmoid turning function from Ex. 3.1. As initial conditions we use the isotropic steady state solutions (9) perturbed by a sine function with period 1. Fig. 6 confirms several assumptions and results from Sec. 5.2: The fractions u_1/u and v_1/v form traveling waves moving in the direction *opposite* of their transport direction and u and v traveling waves moving in their transport direction. All observed speeds are ± 1, as postulated. We further see that u and v appear to be piecewise continuous, whereas u_1/u and v_1/v appear continuous.

Wave Gallery. Fig. 7 shows a gallery of different wave shapes produced by the dynamics for three choices of aging and turning functions. For each case the correct value for r in (31) was determined numerically. We see that the construction gives correct wave shapes even for complicated choices for $\gamma(\rho)$ and $\lambda(\rho)$ and that the wave profiles include growing crests (upper row), falling crests (middle row) and combinations of both (lower row).

7   Conclusion

In this work we have discussed a simple system of four transport-reaction equations, coupled by their nonlinear reaction terms. The system was derived in [8] as an application to the rippling behavior of myxobacteria, but should be interpreted in the larger context of pattern formation in hyperbolic systems ([14, 29]). Despite its simplicity the system's behavior is very rich and we showed that it includes both pulsating-in-time, constant-in-space solutions as well as highly non-trivial counter-propagating traveling waves, whose explicit construction was detailed. The key to uncoupling the two wave frames is the intriguing feature, that the fractions of non-reversing/reversing right-moving densities form traveling waves moving against their transport direction.

Several mathematically and biologically interesting questions arise from this study. The first one concerns the stability of the counter-propagating traveling waves: In the limit of fast-aging two conditions determine the selected wave heights. 1) Linear stability of the individual heights led to an inequality and 2) regularization with a diffusion term yielded an integral condition, which was necessary to fully characterize the wave heights selected in simulations. For the full system (5) both the inequality and the integral condition remain to be found. One expects the inequality condition to be similar or equal to the admissibility condition in Def. 5.3. The numerical results suggest that also an analogue of the the integral condition exists for the full system. Secondly, at this point results about wavelength selection are missing. In [8] it was noted that a diffusion term might be necessary to avoid very short-length waves. As pointed out in [20, 29] linear stability analysis will not be the correct tool to predict wavelengths for such systems, alternative mechanisms for wavelength selection in the memory-free model were discussed in [31], but it remains to be seen if they can be generalized to the 2-age system. Finally it will be interesting to explore if a similar ansatz to decouple wave frames can be used for the continuous-age model (3).

In the class of models discussed here, we examined the feature that the time since the last direction change influences the future behavior of the individual: The organism retains a memory of when it last turned and its subsequent behavior, such as future turning, is influenced by this. Biologically, such a memory effect doesn't need higher brain functions to be realized, it could also be the result of simple biochemistry: biochemical reactions triggered by reversals can influence subsequent behavior, such as the reaction to signaling events (as suggested for myxobacteria e.g. in [19]). This work demonstrates the impact such a memory effect can have on the resulting dynamics.

References

[1] K. Anguige and C. Schmeiser. A one-dimensional model of cell diffusion and aggregation, incorporating volume filling and cell-to-cell adhesion. *J Math Biol*, 58(3):395–427, 2009.

[2] N. Bellomo, A. Bellouquid, J. Nieto, and J. Soler. Multicellular biological growing systems: Hyperbolic limits towards macroscopic description. *Math Models Methods Appl Sci*, 17(supp01):1675–1692, 2007.

[3] M. Burger, V. Capasso, and D. Morale. On an aggregation model with long and short range interactions. *Nonlinear Anal Real World Appl*, 8(3):939–958, 2007.

[4] J. A. Carrillo, M. D'orsogna, and V. Panferov. Double milling in self-propelled swarms from kinetic theory. *Kinet Relat Models*, 2:363–378, 2008.

[5] S. Chapman and T. G. Cowling. *The mathematical theory of non-uniform gases: an account of the kinetic theory of viscosity, thermal conduction and diffusion in gases.* Cambridge university press, 1970.

[6] B. Charlesworth et al. *Evolution in age-structured populations*, volume 2. Cambridge University Press Cambridge, 1994.

[7] P. Degond, A. Manhart, and H. Yu. A continuum model for nematic alignment of self-propelled particles. *Discrete Contin Dyn Syst Ser B*, 22:1295–1327, 2017.

[8] P. Degond, A. Manhart, and H. Yu. An age-structured continuum model for myxobacteria. *Math Models Methods Appl Sci*, https://doi.org/10.1142/s0218202518400043:1–34, 2018.

[9] L. Edelstein-Keshet, J. Watmough, and D. Grunbaum. Do travelling band solutions describe cohesive swarms? An investigation for migratory locusts. *J Math Biol*, 36(6):515–549, 1998.

[10] R. Eftimie. Hyperbolic and kinetic models for self-organized biological aggregations and movement: A brief review. *J Math Biol*, 65(1):35–75, 2012.

[11] R. Eftimie, G. De Vries, and M. Lewis. Complex spatial group patterns result from different animal communication mechanisms. *Proc Natl Acad Sci*, 104(17):6974–6979, 2007.

[12] R. Erban and J. Haskovec. From individual to collective behaviour of coupled velocity jump processes: A locust example. *Kinet Relat Mod*, 5(4):817–842, 2012.

[13] S. Goldstein. On diffusion by discontinuous movements, and on the telegraph equation. *Quart J Mech Appl Math*, 4(2):129–156, 1951.

[14] K. P. Hadeler. Reaction transport systems in biological modelling. In *Mathematics inspired by biology*, pages 95–150. Springer, 1999.

[15] T. Hillen. Hyperbolic models for chemosensitive movement. *Math Models Methods Appl Sci*, 12(07):1007–1034, 2002.

[16] T. Hillen and A. Stevens. Hyperbolic models for chemotaxis in 1-D. *Nonlinear Anal Real World Appl*, 1(3):409–433, 2000.

[17] M. Holcombe, S. Adra, M. Bicak, S. Chin, S. Coakley, A. I. Graham, J. Green, C. Greenough, D. Jackson, M. Kiran, et al. Modelling complex biological systems using an agent-based approach. *Integrat Biol*, 4(1):53–64, 2012.

[18] E. E. Holmes. Are diffusion models too simple? A comparison with telegraph models of invasion. *Am Nat*, 142(5):779–795, 1993.

[19] O. Igoshin, A. Mogilner, R. Welch, D. Kaiser, and G. Oster. Pattern formation and traveling waves in myxobacteria: theory and modeling. *Proc Natl Acad Sci USA*, 98(26):14913–14918, 2001.

[20] O. Igoshin, R. Welch, D. Kaiser, and G. Oster. Waves and aggregation patterns in myxobacteria. *Proc Natl Acad Sci USA*, 101(12):4256–4261, 2004.

[21] M. Kac. A stochastic model related to the telegrapher's equation. *Rocky Mt J Math*, 4(3):497–509, 1974.

[22] E. F. Keller and L. A. Segel. Initiation of slime mold aggregation viewed as an instability. *J Theor Biol*, 26(3):399–415, 1970.

[23] F. Lutscher and A. Stevens. Emerging patterns in a hyperbolic model for locally interacting cell systems. *J Nonlinear Sci*, 12(6):619–640, 2002.

[24] A. Manhart and A. Mogilner. Agent-based modeling in cell biology: case study in cleavage furrow models. *Mol Biol Cell*, 27:3379–84, 2016.

[25] J. D. Meiss. *Differential dynamical systems*, volume 14. Siam, 2007.

[26] A. Mogilner and L. Edelstein-Keshet. A non-local model for a swarm. *J Math Biol*, 38(6):534–570, 1999.

[27] H. G. Othmer, S. R. Dunbar, and W. Alt. Models of dispersal in biological systems. *J Math Biol*, 26(3):263–298, 1988.

[28] K. Pakdaman, B. Perthame, and D. Salort. Dynamics of a structured neuron population. *Nonlinearity*, 23:55, 2009.

[29] I. Primi, A. Stevens, and J. J. Velazquez. Pattern forming instabilities driven by non-diffusive interaction. *Netw Heterog Media*, 8(1):397–432, 2013.

[30] B. Sager and D. Kaiser. Intercellular C-signaling and the traveling waves of Myxococcus. *Genes Dev.*, 8(23):2793–2804, 1994.

[31] A. Scheel and A. Stevens. Wavenumber selection in coupled transport equations. *J Math Biol*, 75(5):1047–1073, 2017.